Geochemistry Geophysics Geosystems G3

Article
Volume 12, Number 9
9 September 2011
Q09004, doi:10.1029/2011GC003692
ISSN: 1525-2027

Published by AGU and the Geochemical Society

Field-based validation of a diagenetic effect on *G. ruber* Mg/Ca paleothermometry: Core top results from the Aegean Sea (eastern Mediterranean)

George Kontakiotis
Department of Historical Geology and Paleontology, Faculty of Geology and Geoenvironment, National and Kapodistrian University of Athens, Athens GR-15784, Greece (gkontak@geol.uoa.gr)

P. Graham Mortyn
Institute of Environmental Science and Technology and Department of Geography, Universitat Autònoma de Barcelona, Barcelona E-08193, Spain

Assimina Antonarakou
Department of Historical Geology and Paleontology, Faculty of Geology and Geoenvironment, National and Kapodistrian University of Athens, Athens GR-15784, Greece

Miguel A. Martínez-Botí
Institute of Environmental Science and Technology, Universitat Autònoma de Barcelona, Barcelona E-08193, Spain

Now at Ocean and Earth Science, National Oceanography Centre, Southampton, University of Southampton, Waterfront Campus, Southampton SO14 3ZH, UK

Maria V. Triantaphyllou
Department of Historical Geology and Paleontology, Faculty of Geology and Geoenvironment, National and Kapodistrian University of Athens, Athens GR-15784, Greece

[1] Recent work across the Mediterranean Sea has illustrated the salinity and overgrowth effects on planktonic foraminiferal Mg/Ca, which potentially confound the use of this as a temperature proxy for paleoceanographic reconstructions. To test and verify these effects, we present new Aegean Sea results which reveal Mg/Ca values that were unreasonably high to be explained by temperature or salinity variations alone, confirming that foraminiferal Mg/Ca is affected by diagenesis. We have specifically targeted *Globigerinoides ruber* (w, *sensu stricto*), from a series of modern core tops spanning a strong sea surface salinity gradient and a minor sea surface temperature range, along a north-south Aegean Sea transect. Scanning Electron Microscopy analyses show that *G. ruber* specimens were covered by microscale euhedral crystallites of inorganic precipitates. This secondary calcite phase seems to be responsible for the anomalously high Mg/Ca ratios and likely formed near the sediment/water interface from $CaCO_3$ supersaturated interstitial seawater. We also have clear evidence of diagenetic alteration in a north-south direction along the Aegean Sea, possibly depending on salinity and calcite saturation state gradients. These observations illustrate the necessity of alternative techniques (e.g., flow-through time resolved analysis or laser ablation inductively coupled plasma mass spectrometry) to potentially overcome these diagenetic issues and develop a more reliable and sensitive temperature proxy in similar subtropical settings characterized by high salinity, excessive evaporation, and restricted circulation.

Components: 8000 words, 6 figures, 3 tables.

Keywords: *G. ruber* (w, sensu stricto); Mg/Ca paleothermometry; calcite saturation state; eastern Mediterranean; high-Mg-calcite diagenetic overgrowths; palaeoceanography.

Index Terms: 4924 Paleoceanography: Geochemical tracers; 4944 Paleoceanography: Micropaleontology (0459, 3030); 4954 Paleoceanography: Sea surface temperature.

Received 10 May 2011; **Revised** 8 July 2011; **Accepted** 9 July 2011; **Published** 9 September 2011.

Kontakiotis, G., P. G. Mortyn, A. Antonarakou, M. A. Martínez-Botí, and M. V. Triantaphyllou (2011), Field-based validation of a diagenetic effect on *G. ruber* Mg/Ca paleothermometry: Core top results from the Aegean Sea (eastern Mediterranean), *Geochem. Geophys. Geosyst.*, *12*, Q09004, doi:10.1029/2011GC003692.

1. Introduction

[2] Over the past decade, the applicability of the planktonic foraminiferal Mg/Ca paleothermometer in (sub)tropical settings, such as the semienclosed Mediterranean Sea, has been of special interest due to their unique characteristics (low productivity, extreme salinities and supersaturated water column) [*Ferguson et al.*, 2008; *Hoogakker et al.*, 2009; *van Raden et al.*, 2011]. Mediterranean foraminiferal Mg/Ca data from warm and salty environments have revealed elevated values that do not reasonably correspond with observed temperatures in the region [*Ferguson et al.*, 2008; *Boussetta et al.*, 2011], using existing calibrations [*Anand et al.*, 2003; *Lea et al.*, 2000]. It is likely that secondary factors may have a large influence on Mg/Ca in such settings. It is important to assess these potential influences on the Mg/Ca proxy and whether they need to be more actively considered in a range of semienclosed basins globally, in order to figure out how accurately the Mg/Ca ratio in foraminiferal calcite reflects the ambient temperature (T).

[3] *Ferguson et al.* [2008] identified the salinity (S) effect in the Mediterranean Sea as one of the major limitations to accurately reconstruct T from *G. ruber* Mg/Ca in the region. However, more recent studies [*Hoogakker et al.*, 2009; *van Raden et al.*, 2011; *Boussetta et al.*, 2011] showed that diagenetic overgrowths exert more control on planktonic foraminiferal Mg/Ca ratios compared to S in the Mediterranean. An example of the potential significance of both these effects is also provided in the present study by data from the Aegean Sea, a region where surface S ranges today between ~35–40 psu and its surface and bottom waters are highly supersaturated with respect to calcite (5–6 and ~3.5 Ω respectively [*Schneider et al.*, 2007]). In this area, little biogeochemical research has been carried out on *G. ruber* (w), especially focused on both diagenetic alteration during early burial and on T-S variations of the upper water column. Given the strong heterogeneity at a local scale on Mg/Ca ratios in the entire Mediterranean Sea [*Boussetta et al.*, 2011], we present new Mg/Ca data from different subbasins of the Aegean Sea and we investigate the cause(s) for the anomalously high Mg/Ca ratios measured on these core top samples. Additionally, we make a novel contribution regarding secondary calcite precipitation and its mechanism, by presenting in detail the major characteristics indicative of the high-Mg diagenetic overgrowth inside and outside of *G. ruber* tests, and their origins. Our study serves as a timely complement to the recent work of *Boussetta et al.* [2011], in which a relevant increase in diagenetic signal from west to east in the Mediterranean Sea was shown for the first time, which could be relevant for similar settings (semienclosed basins, marginal seas) globally.

2. Modern Setting and Studied Species

2.1. The Aegean Sea

[4] The Aegean Sea is a semienclosed basin (Figure 1), which can be divided into two main subbasins, north and south Aegean. The two basins have significantly different hydrographic characteristics, controlled by the exchange of water masses with the Levantine and Black Seas and by the climate contrasts between more humid conditions in the north and semiarid conditions in the south [*Lykousis et al.*, 2002]. The Aegean Sea is particularly sensitive to climate variations compared to the open ocean, due to the spatial distribution of both sea surface T and S [*Poulos et al.*, 1997]. The former ranges between 17 and 23°C (Figure 1b), while the latter ranges from less than 35 psu near the Strait of Dardanelles to more than 39.5 psu in the extreme south (Figure 1c). The most

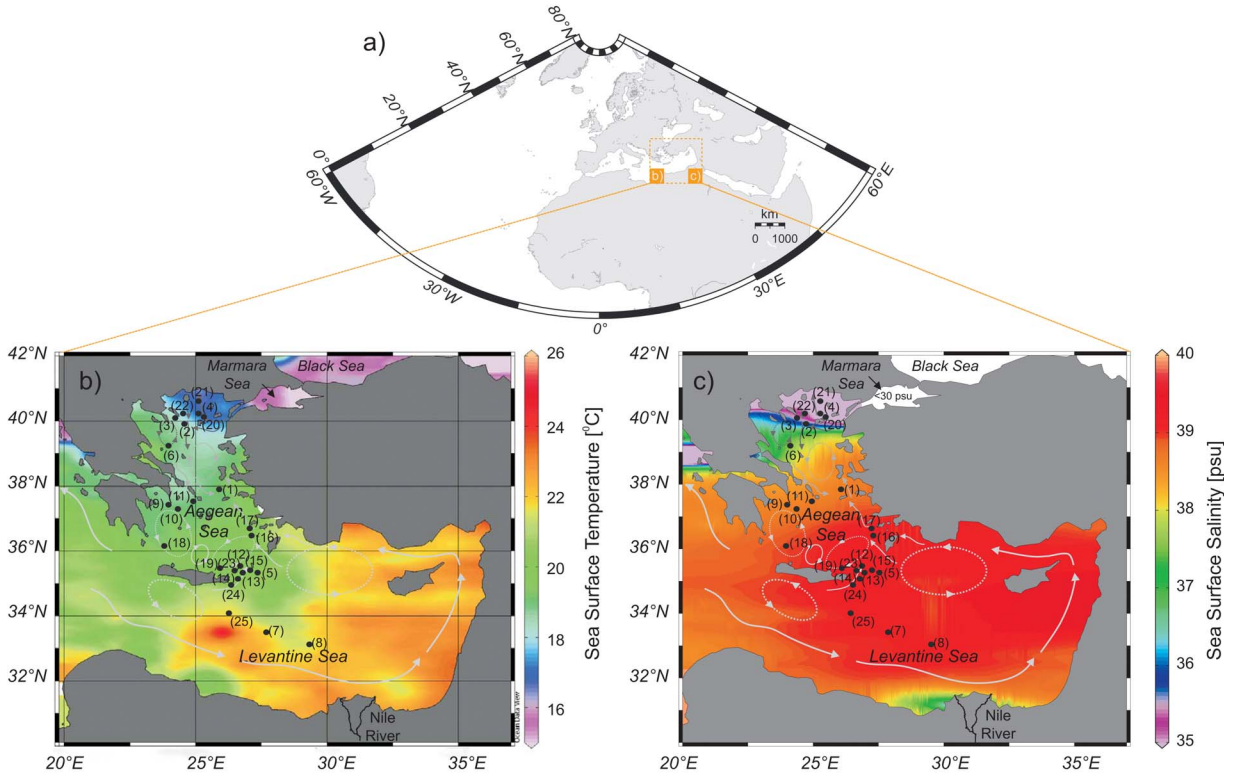

Figure 1. (a) Map of the Mediterranean Sea (modified after *Marino et al.* [2009], copyright 2009, with permission from Elsevier) showing large N-S trends for mean annual (b) sea surface temperature (SST) and (c) sea surface salinity (SSS) in the Aegean region [*Antonov et al.*, 2006]. Shown are the locations of the Aegean sediment cores and the main patterns of the surface circulation (gray arrows), cyclonic (solid circles), and anticyclonic gyres (dashed gray circles) [*Lykousis et al.*, 2002].

pronounced T and S contrasts occur in a N-S direction (Figures 1a–1c and Table 1), with the cooler and fresher waters in the north. These N-S trending T and S gradients in a small geographic area make the Aegean Sea a suitable region for testing combined T and S influences on *G. ruber* Mg/Ca.

2.2. *Globigerinoides ruber*

[5] We have specifically targeted the tropical, spinose planktonic species *G. ruber* (white, *sensu stricto*), which is mainly living in surface oligotrophic waters during its life cycle, due to its symbiotic relationship with photosynthesizing dinoflagellates [*Hemleben et al.*, 1989]. As previous basin-wide [*Farmer et al.*, 2007] or more global [*Lea et al.*, 2000; *Dekens et al.*, 2002] core top studies have highlighted, it constitutes a reliable indicator of mean annual SST conditions in the upper 50 m of the (sub)tropical oceans. This is further supported by the observations of *Pujol and Vergnaud-Grazzini* [1995] particularly for our study region, in which *G. ruber* dominates modern times and develops throughout the year. Among the warm water taxa that have been examined in the Aegean planktonic foraminiferal fauna, for which T and S tolerances are known (14–32°C and 24–47‰ (*G. sacculifer*), 12–31°C and 23–46‰ (*O. universa*) and 11–30°C and 27–45‰ (*G. siphonifera*) [*Bijma et al.*, 1990]), *G. ruber* presents the widest S tolerance range (22–49‰). This double ability to succeed in warm oligotrophic environments, as the Aegean Sea, and to tolerate large S fluctuations, makes this species a promising source of paleoceanographic information and is therefore exclusively utilized here.

3. Materials and Methods

3.1. Site Selection, Sampling, and Age Control

[6] We present *G. ruber* Mg/Ca data from 25 Aegean Sea surface sediment sites, which have been sampled during six expeditions (Table 1). In order to investigate the S and diagenetic overprint influences on the Mg/Ca proxy via the N-S local-scale

Table 1. Core Top Locations, Coordinates, Core Types, Seafloor Water Depths, and Mean Annual T and S Data[a]

Sample Code	Coordinate		Core Type	Ship/Year	Water Depth (m)	SST (°C)	SSS (psu)
	Latitude (°N)	Longitude (°E)					
M51-3-594	37.902.500	26.218.500	multicore	R/V Meteor/2001 (M51–3)	1005	19.75	38.83
M51-3-596	38.954.833	24.753.333	multicore	R/V Meteor/2001 (M51–3)	883	19.03	37.75
M51-3-601	40.088.833	24.611.167	multicore	R/V Meteor/2001 (M51–3)	995	19.00	36.00
M51-3-602	40.217.000	25.240.000	multicore	R/V Meteor/2001 (M51–3)	1496	18.75	35.30
M71-3-Rho 02	35.370.138	27.420.105	multicore	R/V Meteor/2007 (M71–3)	1304	20.55	39.14
M71-3-SK 01	39.330.353	23.480.010	multicore	R/V Meteor/2007 (M71–3)	1267	19.55	36.65
M71-3-Her 01	33.550.440	27.440.444	multicore	R/V Meteor/2007 (M71–3)	2488	21.55	39.17
M71-3-Her 03	29.000.000	33.400.000	multicore	R/V Meteor/2007 (M71–3)	3090	21.39	39.20
C6	37.570.416	24.160.930	gravity core	R/V Hydna/2008	311	19.33	38.55
C18	37.480.198	24.630.561	gravity core	R/V Hydna/2008	257	19.19	38.53
C38	37.620.619	24.950.898	gravity core	R/V Hydna/2008	191	19.15	38.61
M-15-143	35.520.480	26.370.390	gravity core	R/V Aegeo/1998	401	20.25	39.12
M-15-145	35.440.830	26.480.539	gravity core	R/V Aegeo/1998	1402	20.30	39.12
M-15-224	35.340.740	26.310.230	gravity core	R/V Aegeo/1998	1041	20.35	39.13
SL52BC3	35.470.427	27.270.292	box core	R/V Professor Logachev/1998	1316	20.52	39.13
NS-14	36.380.550	27.000.280	gravity core	R/V Aegeo/1998	505	18.52	39.07
NS-40	37.010.130	26.190.040	gravity core	R/V Aegeo/1998	1078	19.78	39.02
MSB4	36.150.010	24.060.380	multicore	R/V Aegeo/1998	914	19.47	38.88
MSB7	35.390.990	26.130.020	multicore	R/V Aegeo/1998	2273	20.30	39.12
MNB5	40.150.000	25.450.000	multicore	R/V Aegeo/1998	520	18.63	35.30
MNB6	40.340.742	25.070.991	multicore	R/V Aegeo/1998	152	18.50	35.25
MNB7	40.160.750	24.500.750	multicore	R/V Aegeo/1998	724	18.95	35.90
M-15-200	35.550.170	26.520.830	gravity core	R/V Aegeo/1998	470.5	20.26	39.11
M-22-17	35.050.600	26.230.070	gravity core	R/V Aegeo/1992	361	20.70	39.15
M71-3-IER 01	34.260.540	26.110.510	multicore	R/V Meteor/2007 (M71–3)	3623	21.54	39.24

[a]Abbreviations are as follows: SST, sea surface temperature; SSS, sea surface salinity. SST and SSS data for each sample were derived from *Antonov et al.* [2006].

gradients, the sampling locations cover all major subbasins in the north and south Aegean Sea. The majority of our study materials are multicore samples with minimal bioturbation influence.

[7] The age of the core top samples has been estimated though linear extrapolation, using the ages of the top of the most recent sapropel S1 (~10.0–6 ka cal BP [*Geraga et al.*, 2000, 2005; *Rohling et al.*, 2002; *Triantaphyllou et al.*, 2009b]) and the Z2 Minoan ash layer in a set of well-dated Aegean sediment records (Table 2) and assuming that the sedimentation rates are constant during the interval post 3550 yr B.P. The latter marker horizon, known as "Mediterranean Minoan tephra Z2," was identified in cores MSB4, MSB7, MNB5, MNB6 [*Giresse et al.*, 2003], NS-14 and NS-40 [*Triantaphyllou et al.*, 2009a] and has been dated between 3550 and 3577 cal years B.P. [*Friedrich et al.*, 2006]. Moreover, the top of S1 has been determined in the majority of the studied cores and its widespread distribution provides an additional chronological marker of the core top sediments. According to *Casford et al.* [2007], given the Aegean's limited area, it is expected that these events would be virtually synchronous across the basin. Additionally, the Late Holocene age is corroborated by core top dates, which are based on the extrapolation of the lithostratigraphy of hemipelagic successions from surrounding cores (marked with an asterisk) and range in age from 150 to 2464 yr B.P. (Table 2). Accordingly, all core tops are suggested to have a modern age and our data set represents an integrated record of some 100 yr to a few ky, at most, depending on the core location. Due to the subrecent character of the analyzed material, we have compared our core top data set with mean annual T and S data from the World Ocean Atlas Climatology 2005 [*Antonov et al.*, 2006]. The annual sea surface T and S for each core site ranges from 18.7°C and 35.3 psu in the north, to 23.0°C and 39.3 psu in the south (Table 1).

3.2. SEM Investigation, Sample Preparation, and Mg/Ca Analysis

[8] Selected samples were subjected to careful inspection by Scanning Electron Microscopy (SEM) to evaluate the physical texture of *G. ruber* tests. Therefore, the inner and outer surfaces of uncleaned (Figure 2), as well as of slightly crushed and ultrasonically cleaned (with ultrapure milliQ water for 30 s) (Figure 3), *G. ruber* specimens were

Table 2. The Chronostratigraphic Framework of the Aegean Core Top Samples[a]

Cores	Location	S1 Depth (cm)	Z2 Depth (cm)	Age (uncal yr B.P.)	Basis	Reference Study
NS-14	south Aegean	S1a: 80–120, S1b: 55–69	17	2464	linear extrapolation	*Triantaphyllou et al.* [2009a]
HCM 2/22*	south Cretan margin	S1a: 24–28.5, S1b: 16–22	10	2044	linear extrapolation	*Katsouras et al.* [2010]
SIN 97-01GC*	south Aegean	22.5–44.5	–	1050 ± 55	^{14}C AMS	*Gennari et al.* [2009]
MSB4	south Aegean	–	22–24	278	linear extrapolation	*Giresse et al.* [2003]
MSB7	south Aegean	–	47	497	linear extrapolation	*Giresse et al.* [2003]
LC-21*	south Aegean	S1a: 130–150, S1b: 162–178	10	≈1300	linear extrapolation	*Rohling et al.* [2002]
C69*	south Aegean	S1a: 35–40, S1b: 26–30	15	1295	linear extrapolation	*Geraga et al.* [2005]
C40*	south Aegean	S1a: 84–96, S1b: 73–78	36	150	linear extrapolation	*Geraga et al.* [2000]
MNB3*	north Aegean	S1a: 144–161, S1b: 128–140	14	1365	linear extrapolation	*Gogou et al.* [2007]
SL-152*	north Aegean	S1a: 302–345, S1b: 272–293	–	1558	linear extrapolation	*Katsouras et al.* [2010]
M3*	north Aegean	S1a: 152–178, S1b: 129–139	–	275	linear extrapolation	*Roussakis et al.* [2004]

[a]Additional cores, based on a combination of calibrated AMS ^{14}C and extrapolated datings, are marked with an asterisk.

gold coated and photographed using SEM. Additionally, 15–20 *G. ruber* specimens from each sample were photographed in order to trace the type and the degree of the diagenetic alteration. High-resolution SEM analyses were performed at the National and Kapodistrian University of Athens (Department of Historical Geology-Paleontology) with a Jeol JSM 6360 SEM.

[9] Between 20 and 35 specimens were picked from each sample within the 250–355 μm size fraction (approximately 200–350 μg of calcite). This approach averages the T signal recorded by individual tests comprising the sample population [*Barker et al.*, 2003; *Anand and Elderfield*, 2005]. Prior to cleaning and under microscopic view, the shells were gently crushed, using methanol-cleaned glass plates, to ensure that all chambers were opened without pulverizing the sample, and the samples were loaded into acid-cleaned microvials. The cleaning procedure followed the "Cd method"

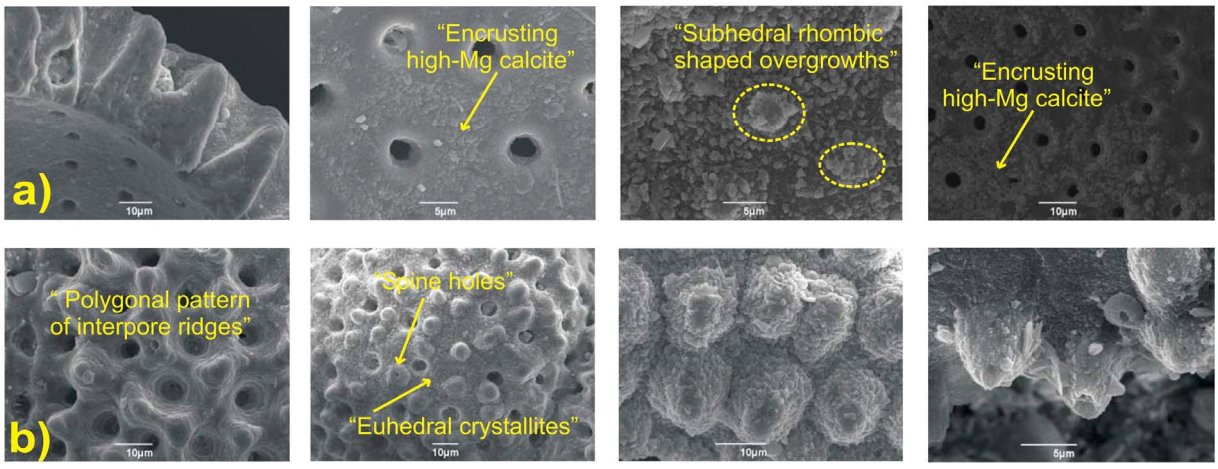

Figure 2. High-resolution SEM images of uncleaned *G. ruber* tests from Aegean Sea showing their (a) internal structure and (b) characteristic surface morphology. Both the interior and the exterior of the specimens show the presence of encrusting high-Mg calcite, containing subhedral, rhombic-shaped euhedral crystallites. The thick chamber wall can be seen in the broken edge of the last chamber, while the magnified view of the exterior shows the well-developed polygonal pattern of interpore ridges by calcite plaque deposition on the smooth chamber surface. Scale bars are indicated on each image.

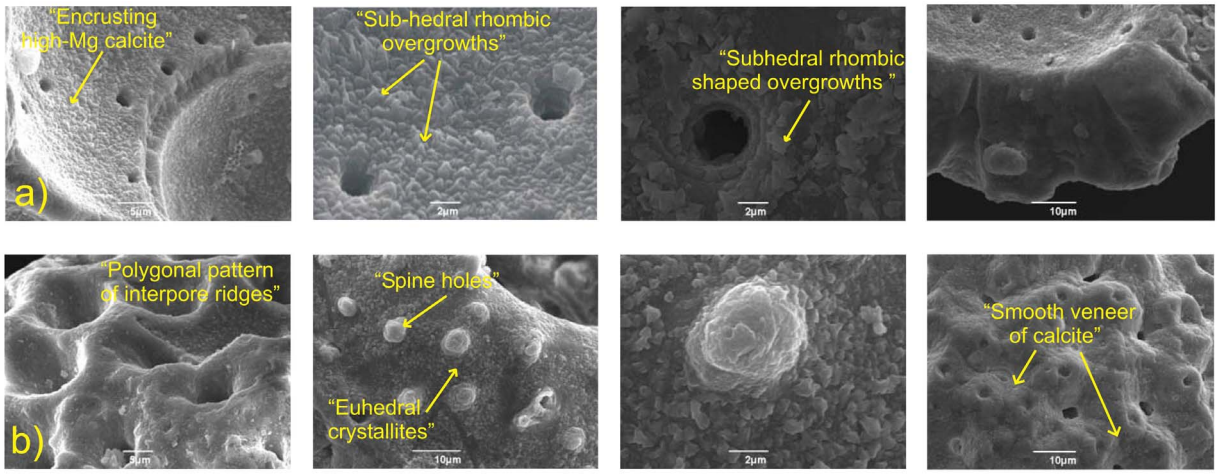

Figure 3. High resolution SEM images of cleaned (slightly crushed and sonicated, see text) *G. ruber* tests from Aegean Sea showing their (a) internal structure and (b) characteristic surface morphology. Both are indicative of secondary inorganic high-Mg calcite overgrowths. The enlargement of different parts of the test exterior shows a well-developed polygonal pattern of interpore ridges, formed by flat calcite plaques during ontogenetic calcification, the euhedral crystallites and the spine holes, which collectively increase topography on the outer surface of the tests. In heavily overgrown specimens the strong diagenetic overprint can clearly be seen (smooth veneer of calcite), almost closing off the pore pits and obscuring the interpore ridges. The wall surface textures of opened *G. ruber* chambers also show subhedral rhombic shaped overgrowths. Scale bars are indicated on each image.

[*Rosenthal et al.*, 2004], which involves a number of discrete sequential steps with the objective of removing various contaminant phases: (a) clay materials, (b) Fe-Mn oxide coatings (which could be a contamination source associated with reducing conditions in the eastern Mediterranean), and (c) organic matter.

[10] Foraminiferal trace element cleaning procedures were performed at the Universitat Autònoma de Barcelona (UAB) and Mg/Ca ratios were analyzed by Inductively Coupled Plasma Mass Spectrometer (ICP-MS), also at the UAB. The samples were measured against a set of multielemental standard solutions prepared from single-element primary standards and matrix matched to 40 ppm Ca. The long-term reproducibility of the Mg/Ca analyses yielded precisions of 1.9%, based on repeated analysis of two consistency standards (n = 74) with variable metal/Ca ratios to mimic the natural variations in foraminifera.

4. Results

4.1. Compilation of Core Top Data

[11] Mg/Ca data are summarized in Table 3 and are significantly higher, for the same T, than those data seen in other regions beyond the Mediterranean. Moreover, as previously observed in core top databases from the Mediterranean [*Ferguson et al.*, 2008; *Boussetta et al.*, 2011], Mg/Ca ratios show a large variability with values ranging from 3.35 to 21.61 mmol/mol with a mean value of 12.48 mmol/mol (Table 3). No significant relationship between Mg/Ca and Fe/Ca or Mn/Ca was observed, and the latter trace metal ratios remained below the contamination threshold values of 175 μmol/mol [*Boyle*, 1983] and 100 μmol/mol [*Barker et al.*, 2003] respectively, in all samples. Although 22 of the 25 analyzed samples display Al/Ca values above the threshold limit of 40 μmol/mol [*Bice et al.*, 2005], this ratio cannot be used to selectively exclude Mg/Ca data in this setting due to the absence of any relationship between Al/Ca and Mg/Ca ratios, as *Ferguson et al.* [2008] have already shown for the Mediterranean. Mg/Ca ratios were converted to T based on the species-specific calibrations of *Anand et al.* [2003] and *Kısakürek et al.* [2008] for *G. ruber*, presenting values between 23.8°C and 44.5°C and 21.8°C and 44.1°C respectively, with a mean of 34.1°C or 32.9°C, which exceeds the upper T tolerance of *G. ruber* [*Bijma et al.*, 1990]. In both cases, the average calculated Ts are too high to be realistic as they are 12.9–14.1°C higher than the recent average annual SST of 20°C in the Aegean Sea.

Table 3. Observed, Predicted, and Residual Mg/Ca Ratios for *G. ruber* Samples[a]

Core Tops	Observed Mg/Ca	Predicted Mg/Ca[b]	Residual Mg/Ca[b]	Predicted Mg/Ca[c]	Residual Mg/Ca[c]
M51-3-594	3.65	2.34	1.31	3.03	0.62
M51-3-596	3.36	2.19	1.17	2.68	0.67
M51-3-601	3.91	2.18	1.73	2.41	1.50
M51-3-602	3.51	2.14	1.37	2.27	1.24
M71-3-Rho 02	6.69	2.51	4.18	3.29	3.40
M71-3-SK 01	3.53	2.29	1.24	2.62	0.91
M71-3-Her 01	10.39	2.75	7.64	3.58	6.82
M71-3-Her 03	8.23	2.71	5.52	3.53	4.69
C6	15.28	2.25	13.03	2.88	12.39
C18	13.06	2.22	10.84	2.85	10.22
C38	9.96	2.21	7.75	2.85	7.11
M-15-143	11.69	2.44	9.25	3.21	8.48
M-15-145	16.02	2.46	13.57	3.23	12.80
M-15-224	8.30	2.47	5.84	3.24	5.06
SL52BC3	6.25	2.50	3.75	3.29	2.97
NS-14	6.90	2.09	4.81	2.79	4.11
NS-40	9.30	2.34	6.96	3.07	6.23
MSB4	6.62	2.28	4.34	2.97	3.64
MSB7	4.75	2.45	2.29	3.22	1.52
MNB5	5.23	2.11	3.12	2.24	2.98
MNB6	5.94	2.09	3.85	2.21	3.72
MNB7	4.72	2.17	2.55	2.39	2.33
M-15-200	21.61	2.45	19.16	3.21	18.40
M-22-17	14.30	2.54	11.75	3.34	10.96
M71-3-IER 01	4.72	2.74	1.98	3.59	1.14

[a]Residual Mg/Ca is the observed Mg/Ca minus predicted Mg/Ca. The latter has been calculated using the calibrations of *Anand et al.* [2003] and *Kısakürek et al.* [2008].
[b]*Anand et al.* [2003].
[c]*Kısakürek et al.* [2008].

4.2. SEM Observations

[12] Scans of *G. ruber* tests (Figures 2 and 3) were performed after the SEM cleaning step (see section 3.2) and confirm that for the majority of the analyzed specimens much of the test does not consist of calcite formed during ontogenesis, but of postdepositional calcite with signs of early burial diagenesis. Investigations at higher magnification clearly confirm that the inner (Figures 2a and 3a) and outer (Figures 2b and 3b) surfaces of *G. ruber* tests were regularly covered by crystalline syntaxial overgrowth with rhombohedral crystal terminations. The size of the single crystals amounts to 2–5 μm. The overgrowth is more evident outside foraminiferal chambers, where crystals appear euhedral and grow in clusters developing outward from the external wall and producing a smooth veneer of calcite (Figure 3b). Particularly on samples from the south Aegean (S > 38 psu), external surfaces are more highly overgrown with microscale euhedral crystallites, which cover the outer ridges and sometimes narrow the pores, filling them at their insides or almost closing them (Figure 3b). A magnified view of the exterior also shows the euhedral crystallites and the spine holes to develop between a well-developed polygonal pattern of interpore ridges (Figures 2b and 3b), which is indicative of *G. ruber* architecture [*Sexton et al.*, 2006]. Although the discarding of spines or the presence of euhedral calcite could be considered as a sign of gametogenesis, there is evidence that *G. ruber* does not add gametogenic calcite of any thickness [*Ni et al.*, 2007].

5. Discussion

5.1. Mg/Ca-T Relationship

[13] The plot of Mg/Ca versus mean annual SSTs (Figure 4) shows that Mg/Ca ratios are higher than what can be expected from Mg/Ca-T calibrations based both on open ocean core tops [*Lea et al.*, 2000] and sediment traps [*Anand et al.*, 2003], and furthermore that they are scattered with a very low correlation to T (R^2 = 0.10). Aegean Mg/Ca ratios are close to those obtained by *Boussetta et al.* [2011], while they show a significant discrepancy from those of *Ferguson et al.* [2008] (similarly to that observed in Levantine Basin where S exceeds 38.5 psu). This deviation is not surprising, since the

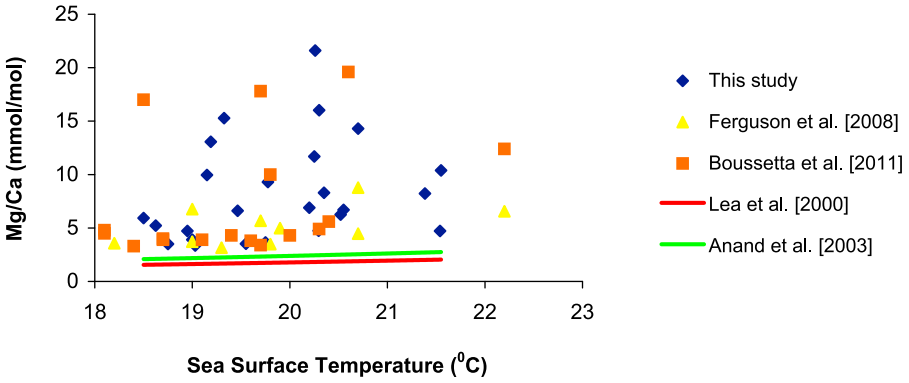

Figure 4. *G. ruber* (w) Mg/Ca versus sea surface temperature (SST) [*Antonov et al.*, 2006]. Aegean core tops are symbolized by blue diamonds, while additional Mediterranean core tops are shown as yellow triangles [*Ferguson et al.*, 2008] and orange squares [*Boussetta et al.*, 2011]. The red and green curves are the exponential regressions of *Lea et al.* [2000] and *Anand et al.* [2003], respectively. The scattered Mg/Ca data for all the Mediterranean show the poor relationships between Mg/Ca and SST.

majority of the samples analyzed in *Ferguson et al.* [2008] come from the western and central Mediterranean, presenting lower Mg/Ca values. Temperature has a noticeable effect, but the low regression coefficient suggests that other factor(s) also affect the *G. ruber* Mg/Ca ratio in this region.

5.2. Assessing Other Potential Influences on *G. ruber* Mg/Ca

[14] Considering that our samples were collected from a variety of subbasins, there are many possible factors, other than T, which could potentially affect the Mg/Ca ratios. Accounting for potential artifacts, we first assess the impact of carbonate ion concentration. Additionally, we present sensitivity analyses to the S and the overgrowth effect in order to provide reasonable constraints on uncertainties associated with Mg/Ca-based T.

5.2.1. Carbonate Ion Concentration

[15] A plausible candidate for the high Mg/Ca values is the variation in carbonate ion concentration ($[CO_3^{2-}]$) during *G. ruber* calcification. Although the distribution of alkalinity in eastern Mediterranean Sea is difficult to determine due to the spatially and temporally limited measurements [*Schneider et al.*, 2007], three lines of evidence add confidence that our high Mg/Ca ratios could not be attributed to the carbonate ion effect. The estimated $[CO_3^{2-}]$ values in the Aegean Sea (241–375 μmol/kg [*Triantaphyllou et al.*, 2010]) are inside the range observed in the entire Mediterranean Sea (170–300 μmol/kg (E. A. Boyle, Carbcalc 5e, 2005, available at http://boyle.mit.edu/~ed/miscellaneous.html)) and in the open ocean (110–280 μmol/kg [*Russell et al.*, 2004]). Second, planktonic foraminiferal Mg/Ca ratios have been shown to be constant, or even to decrease, when $[CO_3^{2-}] > 200$ μmol/kg [*Russell et al.*, 2004]. Finally, according to the calculations of *Kısakürek et al.* [2008] on cultured *G. ruber* from the Red Sea, $[CO_3^{2-}]$ has no effect on Mg/Ca values between S values of 32 and 41 psu.

5.2.2. Salinity

[16] In order to examine the S influence, we calculated the predicted and residual Mg/Ca for our samples. The predicted Mg/Ca is obtained using the equations of *Anand et al.* [2003] and *Kısakürek et al.* [2008]. The residual Mg/Ca is the observed minus the predicted value and represents the excess T-independent *G. ruber* Mg/Ca variability. Predicted *G. ruber* Mg/Ca values are generally much lower than observed ones (Table 3).

[17] Our residual Mg/Ca values do not exhibit a significant correlation with mean annual SSS ($R^2 = 0.19$) (Figure 5). The comparison with other Mediterranean core tops [*Ferguson et al.*, 2008; *Boussetta et al.*, 2011] shows similarly wide scatter, especially at high values (Aegean and Levantine regions), which cannot be easily attributed to S alone. This differs markedly from core tops retrieved at lower open ocean salinities ($32.6 < S < 37$ psu [*Mathien-Blard and Bassinot*, 2009]; $35.6 < S < 37.3$ psu [*Arbuszewski et al.*, 2010]), where the residual Mg/Ca seems to be correlated with SSS. However, those data sets do not include samples from $S > 37.3$ psu and therefore we cannot directly compare our results in the same S range. At

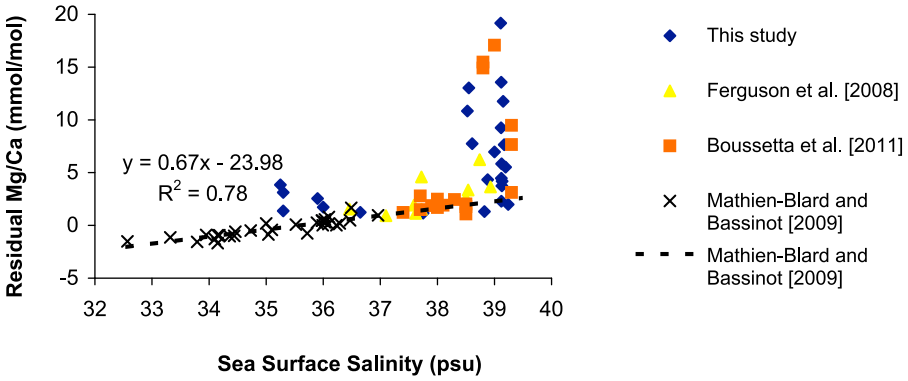

Figure 5. Residual Mg/Ca (observed Mg/Ca minus predicted Mg/Ca, see text) versus sea surface salinity (SSS) [*Antonov et al.*, 2006]. Aegean core tops are symbolized by blue diamonds, while other Mediterranean core tops are shown as yellow triangles [*Ferguson et al.*, 2008] and orange squares [*Boussetta et al.*, 2011]. The black dashed curve is the linear regression equation obtained by *Mathien-Blard and Bassinot* [2009].

S > 38.5 psu, most of our measurements depart from the empirical regression line of *Mathien-Blard and Bassinot* [2009] and show that in such high salinity environments there is an additional contribution that leads the Mg/Ca ratio to ultrahigh values.

5.2.3. Diagenetic Influence on Mg/Ca

[18] A persistent problem in many paleoceanographic studies is the potential for diagenetic processes to compromise the fidelity of geochemical proxies on microfossils, such as foraminifera. Planktonic foraminifera are especially sensitive to such chemical alteration [*Sexton et al.*, 2006]. Inorganic/diagenetic calcite, in the form of overgrowths, may mask the primary oceanographic signal of planktonic foraminiferal tests and substantially bias the resultant Mg/Ca ratios to more positive values [*Regenberg et al.*, 2007; *Boussetta et al.*, 2011]. Due to inorganic calcite containing about an order of magnitude more Mg than planktonic foraminiferal calcite [*Mucci*, 1987], only a small amount of overgrowth remaining on the foraminiferal test after the Mg-cleaning procedure would be sufficient to raise the Mg/Ca ratio of the sample calcite [*Regenberg et al.*, 2007]. Such inorganic calcite can be easily distinguished from the biogenic calcite because it consists of large, equant in size and shape crystals, often growing inward or outward from the test surface with radially directed c axes [*Crudeli et al.*, 2004]. According to *Hover et al.* [2001], during early diagenesis in pore waters original biogenic crystallites are transformed via inorganic crystal growth processes which act to lower the surface free energy of crystallites by producing more equant and larger crystals. Particularly in the case of high-Mg calcite, its elongated rhombohedral crystal habits become more equant in shape by dissolution at tips of grains and by precipitation on the planar crystal surfaces.

5.2.3.1. Control of High-Mg Calcite on the Aegean Diagenetic Overgrowths

[19] An unusual feature of the eastern Mediterranean sediments is that they contain both the less (low-Mg calcite) and the more (high-Mg calcite) soluble $CaCO_3$ polymorphs [*Thomson et al.*, 2004]. Especially the latter is usually found in sediments below waters where the carbonate system is oversaturated, and therefore the high-Mg calcites found in the eastern Mediterranean marls are believed to be diagenetic [*Calvert and Fontugne*, 2001]. Additionally, the well-mixed water column in the eastern Mediterranean basin has a T > 12.5°C [*Klein et al.*, 1999], so that the high-Mg calcite is favored to precipitate in sediments [*Morse et al.*, 1997]. The geochemical fingerprint of this alteration, crystallites with high-Mg concentrations, has been observed on planktonic foraminiferal tests from different subbasins (Ionian, Levantine basins) of the eastern Mediterranean Sea (~10% Mg [*Ferguson et al.*, 2008]; 10–12% Mg [*Boussetta et al.*, 2011]).

[20] In the case of the oversaturated Aegean basin, *Triantaphyllou et al.* [2010] have documented overcalcification on living coccospheres of *Emiliania huxleyi* coccoliths during winter season, possibly due to supersaturation of the water column. This could be interpreted as evidence

of overgrowth initiation, even within the water column, and agrees well with the previously published strong diagenetic effect on the same species from eastern Mediterranean sediments [*Crudeli et al.*, 2004]. These observations reinforce our assumption for the presence of high-Mg overgrowths also impacting our *G. ruber* tests. The water column is supersaturated with respect to calcite throughout the year ($5.5 < \Omega < 8.6$ [*Triantaphyllou et al.*, 2010]), and pore waters at and just below the seafloor have been saturated with respect to Mg calcite for at least the past 14000 years [*Cita et al.*, 1977], suggesting that diagenetically induced high-Mg precipitation caused the observed overgrowths.

5.2.3.2. Mechanism of the Diagenetic Influence: Correlation Between Salinity and Calcite Saturation State

[21] Although it is difficult to pinpoint the true mechanism causing the observed overgrowths, it is most likely related to the degree of saturation of the water column. The saturation mechanism was proposed by *van Raden et al.* [2011] for the central Mediterranean, and verified by *Boussetta et al.* [2011] for the entire Sea (expressed mostly in Levantine Basin); thus it is logical to invoke it here for the Aegean Sea.

[22] In hypersaline basins like the Aegean, relatively high T and S values are expected to produce waters supersaturated with respect to $CaCO_3$ and hence promote the precipitation of inorganic calcite. In particular, the warm and salty bottom waters in the south Aegean have a very high saturation state, meaning that the number of ions increases, which results in a higher ionic strength but also in a decrease of their activity [*van Raden et al.*, 2011]. These disproportional activities for the different ions in the carbonate system are directly represented by the absolute [CO_3^{2-}] values and indirectly by the saturation state of seawater [*Raitzsch et al.*, 2010] and the rate of calcite precipitation [*Dueñas-Bohórquez et al.*, 2009]. Consequently, the S increase combined with highly saturated conditions in the Aegean Sea lead to a faster rate of Mg^{2+} substitution for Ca^{2+} in calcite. Despite the fact that these cations have similar electrochemical characteristics, the relatively small ionic radius of Mg^{2+} severely distorts the sixfold coordinated calcite lattice and favors the creation of a new one, which is characterized by a higher average Mg^{2+} density and is represented by the occurrence of high-Mg overgrowths [*Zhang and Dawe*, 2000]. The absence or their minor contribution in the north Aegean Sea is likely linked to its lower saturation state, due to the higher freshwater runoff from the Black Sea.

[23] Our observations seem to confirm a strong link between the water column carbonate composition and salinity of the interstitial waters and the production of diagenetic high-Mg overgrowths on *G. ruber*. According to this scenario, the absence of secondary precipitations in the less saline open ocean [*Arbuszewski et al.*, 2010] could be attributed to the fact that deep waters in the open ocean are either undersaturated (when dissolution occurs) or only slightly oversaturated (Ω just over 1).

5.2.3.3. Assessing the Extent of Diagenetic Alteration and Its Paleoceanographic Implications

[24] The mode of diagenetic alteration presumably depends on many factors, including time, water depth, burial history, sediment composition, burial temperature, pore water chemistry, and crystallography/morphology of foraminifer shells [*Regenberg et al.*, 2007; *Boussetta et al.*, 2011]. Detailed inspection of overgrowths on *G. ruber* specimens is a powerful tool to trace the type and degree of diagenetic modifications, as well as to interpret the associated high Mg/Ca ratios.

[25] In our samples we have clear evidence that *G. ruber* are differentially affected by carbonate diagenesis in the Aegean Sea (Figure 6). In the case of samples with $35 < S < 37$ psu (north Aegean), overgrowth effects are less apparent in the final chamber (Figures 6a and 6b), displaying slightly overgrown specimens. At $37 < S < 38.5$ psu (subbasins between north and south Aegean), secondary precipitates are observed in clusters and gradually in the whole periphery of the tests (Figures 6c and 6d). We frequently observe that the number and extent of these high-Mg outgrowing overgrowths decrease with chamber position in the final whorl, since they mostly occur parallel to the aperture (Figure 6d). The gradual diagenetic increase in a N-S direction is more evident in the south Aegean ($38.5 < S < 39.5$ psu), where *G. ruber* specimens show a distinct additional layer on their outer surface, which is comprised by large, well-developed euhedral crystals, typical of heavily overgrown specimens (Figures 6e and 6f).

[26] Evidences of more massive overgrown specimens in the Aegean Sea compared to those observed in the Red Sea [*Hoogakker et al.*, 2009] could probably be the cause of our higher Mg/Ca ratios (maximum 19.6 and 13.0 mmol/mol,

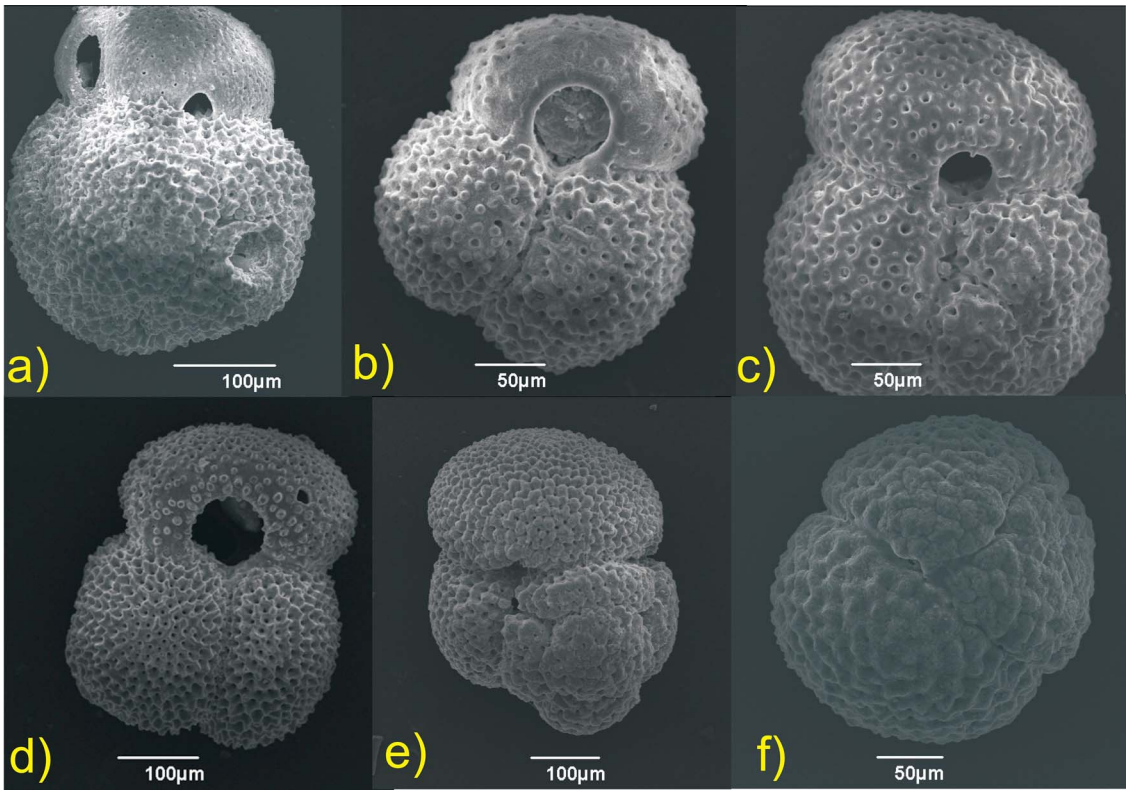

Figure 6. SEM images of Aegean *G. ruber* tests showing the gradually outgrowing overgrowths from (a and b) slightly (35 < S < 37 psu), (c and d) moderately (37 < S < 38.5 psu), and (e and f) heavily overgrown specimens (38.5 < S < 39.5 psu). Scale bars are indicated on each image.

respectively). A possible reason for both the more active diagenetically driven enrichment in Mg and the more extensive overgrowth effects encountered in the Aegean Sea could be the different degree of carbonate dissolution and precipitation, as well as the degree of calcite supersaturation between the basins. The maximum saturation state was found at $36.5 \leq S \leq 40$ psu, due to the rapid decrease in alkalinity in such settings [*Zhong and Mucci*, 1989]. Furthermore, the carbonate removal and precipitation, relative to S change, had been found to be faster in waters with $36.5 \leq S \leq 40$ psu than in extremely high salinity waters ($S \geq 40$ psu) [*Morse et al.*, 1984]. Indeed, the most recent available data [*Triantaphyllou et al.*, 2010] for the Aegean carbonate system (in a N-S direction) have revealed Ω calcite values ranging from 5.5 to 8.6. This scenario is also supported by the fact that the diagenetic alteration of periplatform deposits, such as those of the Aegean, is a more rapid and extensive process relative to monopelagic deep-sea sediments, because these metastable phases (e.g., high-Mg calcite) have a higher diagenetic potential [*Melim et al.*, 2002].

[27] Overall, the results contribute to our understanding of the complexities of the Mg/Ca proxy in the Aegean Sea (eastern Mediterranean) and highlight that accurate reconstruction of SSTs hinges on our ability not only to identify but to also quantify the amount of diagenetic overprint. We therefore suggest that a microanalytical approach, such as flow-through time resolved analysis (FT-TRA) [e.g., *Boussetta et al.*, 2011] or Laser Ablation Inductively Coupled Plasma Mass Spectrometry (LA-ICPMS) [e.g., *Hoogakker et al.*, 2009], must be used to delineate the pure foraminiferal calcite Mg/Ca signal from that of inorganic high-Mg calcite, such that use of diagenetically compromised foraminiferal shells will lead to a sensitive T proxy in similar subtropical settings characterized by high salinity, excessive evaporation, and restricted circulation.

6. Conclusions

[28] The *G. ruber* Mg/Ca ratio data set from a N-S core top transect along the Aegean Sea supplemented with SEM analyses allows us to directly

observe the precipitation of high–Mg calcite overgrowths and to address the anomalously high Mg/Ca ratios. The diagenetic overgrowth effect provides an explanation for why the magnitude of planktonic foraminiferal Mg/Ca in the eastern Mediterranean may differ from their counterparts in other regions (e.g., open ocean). Our results show that:

[29] 1. *G. ruber* Mg/Ca appears anomalously high relative to in situ SSTs and those predicted using open ocean Mg/Ca-T calibrations.

[30] 2. These elevated values correlate poorly with SST and SSS, indicating that they cannot be explained by T or S variations alone. The primary oceanographic signal is masked by the diagenetic processes through the precipitation of high–Mg calcite overgrowths.

[31] 3. The first field-based evidence of overgrowth effect on foraminiferal Mg/Ca ratios from the Aegean Sea emphasizes the key role that carbonate saturation state has on early diagenesis of *G. ruber* calcite and demonstrates how effective this overprint is at increasing Mg/Ca ratios, such that only when it is accounted for in such environments can the paleothermometer be potentially more reliable.

[32] 4. SEM evidence supports the general trend to stronger diagenetic overprint in the south Aegean (S > 38.5 psu). The unique features of the Aegean setting, particularly its semienclosed nature and high salinity, in combination with the different degree of carbonate dissolution/precipitation and the degree of calcite supersaturation between the subbasins, could be the most plausible explanation for the observed N-S diagenetic alteration.

Acknowledgments

[33] The authors are grateful to Laura Rodríguez Sanz and Ignacio Villarroya for kind assistance during the trace element analyses. Special thanks are due to K.-C. Emeis, G. Anastasakis and A. Gogou for providing part of the study material. Elisa Malinverno is warmly thanked for her constructive suggestions during field work, and Margarita Dimiza is thanked for assistance and technical support during SEM analyses. Constructive comments by two anonymous reviewers and Editor Joel A. Baker have been essential in improving the manuscript. We also thank the Erasmus bilateral collaboration between University of Athens and the Autonomous University of Barcelona (ICTA). This research has been financially supported by IAS 2007 postgraduate grant to George Kontakiotis and various lines of Spanish Ministry of Science and Innovation support (including grant CTM2006-11936) to P.G.M. and M.A.M.B.

References

Anand, P., and H. Elderfield (2005), Variability of Mg/Ca and Sr/Ca between and within the planktonic foraminifers *Globigerina bulloides* and *Globorotalia truncatulinoides*, *Geochem. Geophys. Geosyst.*, *6*, Q11D15, doi:10.1029/2004GC000811.

Anand, P., H. Elderfield, and M. H. Conte (2003), Calibration of Mg/Ca thermometry in planktonic foraminifera from a sediment trap time series, *Paleoceanography*, *18*(2), 1050, doi:10.1029/2002PA000846.

Antonov, J. I., R. A. Locarnini, T. P. Boyer, A. V. Mishonov, and H. E. Garcia (2006), *World Ocean Atlas 2005*, vol. 2, *Salinity*, *NOAA Atlas NESDIS*, vol. 62, edited by S. Levitus, 182 pp., NOAA, Silver spring, Md.

Arbuszewski, J., P. deMenocal, A. Kaplan, and E. C. Farmer (2010), On the fidelity of shell-derived $\delta^{18}O_{seawater}$ estimates, *Earth Planet. Sci. Lett.*, *300*, 185–196, doi:10.1016/j.epsl.2010.10.035.

Barker, S., M. Greaves, and H. Elderfield (2003), A study of cleaning procedures used for foraminiferal Mg/Ca paleothermometry, *Geochem. Geophys. Geosyst.*, *4*(9), 8407, doi:10.1029/2003GC000559.

Bice, K., G. Layne, and K. Dahl (2005), Application of secondary ion mass spectrometry to the determination of Mg/Ca in rare, delicate, or altered planktonic foraminifera: Examples from the Holocene, Paleogene, and Cretaceous, *Geochem. Geophys. Geosyst.*, *6*, Q12P07, doi:10.1029/2005GC000974.

Bijma, J., W. W. Faberand, and C. Hemleben (1990), Temperature and salinity limits for growth and survival of some planktonic foraminifers in laboratory cultures, *J. Foraminiferal Res.*, *20*, 95–116, doi:10.2113/gsjfr.20.2.95.

Boussetta, S., F. Bassinot, A. Sabbatini, N. Caillon, J. Nouet, N. Kallel, H. Rebaubier, G. Klinkhammer, and L. Labeyrie (2011), Diagenetic Mg-rich calcite in Mediterranean sediments: Quantification and impact on foraminiferal Mg/Ca thermometry, *Mar. Geol.*, *280*, 195–204, doi:10.1016/j.margeo.2010.12.011.

Boyle, E. A. (1983), Manganese carbonate overgrowths on foraminiferal tests, *Geochim. Cosmochim. Acta*, *47*, 1815–1819, doi:10.1016/0016-7037(83)90029-7.

Calvert, S. E., and M. R. Fontugne (2001), On the late Pleistocene-Holocene sapropel record of climatic and oceanographic variability in the eastern Mediterranean, *Paleoceanography*, *16*(1), 78–94, doi:10.1029/1999PA000488.

Casford, J. S. L., R. H. Abu-Zied, E. J. Rohling, S. Cooke, C. Fontanier, M. Leng, A. Millard, and J. Thomson (2007), A stratigraphically controlled multiproxy chronostratigraphy for the eastern Mediterranean, *Paleoceanography*, *22*, PA4215, doi:10.1029/2007PA001422.

Cita, M. B., C. Vergnaud-Grazzini, D. Robert, H. Chamley, N. Ciaranfi, and S. D'Onofrio (1977), Paleoclimatic record of a long deep-sea core from the eastern Mediterranean, *Quat. Res.*, *8*, 205–235, doi:10.1016/0033-5894(77)90046-1.

Crudeli, D., J. R. Young, E. Erba, G. J. de Lange, K. Henriksen, H. Kinkel, C. P. Slomp, and P. Ziveri (2004), Abnormal carbonate diagenesis in Holocene-late Pleistocene sapropel-associated sediments from the eastern Mediterranean; Evidence from *Emiliania huxleyi* coccolith morphology, *Mar. Micropaleontol.*, *52*, 217–240, doi:10.1016/j.marmicro.2004.04.010.

Dekens, P. S., D. W. Lea, D. K. Pak, and H. J. Spero (2002), Core top calibration of Mg/Ca in tropical foraminifera:

Refining paleotemperature estimation, *Geochem. Geophys. Geosyst.*, *3*(4), 1022, doi:10.1029/2001GC000200.

Dueñas-Bohórquez, A., R. E. da Rocha, A. Kuroyanagi, J. Bijma, and G.-J. Reichart (2009), Effect on salinity and seawater calcite saturation state on Mg and Sr incorporation in cultured planktonic foraminifera, *Mar. Micropaleontol.*, *73*, 178–189, doi:10.1016/j.marmicro.2009.09.002.

Farmer, E. C., A. Kaplan, P. B. de Menocal, and J. Lynch-Stieglitz (2007), Corroborating ecological depth preferences of planktonic foraminifera in the tropical Atlantic with the stable oxygen isotope ratios of core top specimens, *Paleoceanography*, *22*, PA3205, doi:10.1029/2006PA001361.

Ferguson, J. E., G. M. Henderson, M. Kucera, and R. E. M. Rickaby (2008), Systematic change of foraminiferal Mg/Ca ratios across a strong salinity gradient, *Earth Planet. Sci. Lett.*, *265*, 153–166, doi:10.1016/j.epsl.2007.10.011.

Friedrich, W. L., B. Kromer, M. Friedrich, J. Heinemeier, T. Pfeiffer, and S. Talamo (2006), Santorini eruption radiocarbon dated to 1627–1600 B.C, *Science*, *312*(5773), 548, doi:10.1126/science.1125087.

Gennari, G., F. Tamburini, D. Ariztegui, I. Hajdas, and S. Spezzaferri (2009), Geochemical evidence for high-resolution variations during deposition of the Holocene S1 sapropel on the Cretan Ridge, eastern Mediterranean, *Palaeogeogr. Palaeoclimatol. Palaeoecol.*, *273*, 239–248, doi:10.1016/j.palaeo.2008.06.007.

Geraga, M., S. Tsaila-Monopolis, C. Ioakim, G. Papatheodorou, and G. Ferentinos (2000), Evaluation of palaeoenvironmental changes during the last 18,000 years in the Myrtoon basin, SW Aegean Sea, *Palaeogeogr. Palaeoclimatol. Palaeoecol.*, *156*, 1–17.

Geraga, M., S. Tsaila-Monopolis, C. Ioakim, G. Papatheodorou, and G. Ferentinos (2005), Short-term climate changes in the southern Aegean Sea over the last 48000 years, *Palaeogeogr. Palaeoclimatol. Palaeoecol.*, *220*, 311–332, doi:10.1016/j.palaeo.2005.01.010.

Giresse, P., R. Buscail, and B. Charrière (2003), Late Holocene multisource material input into the Aegean Sea: Depositional and post-depositional processes, *Oceanol. Acta*, *26*, 657–672, doi:10.1016/j.oceact.2003.09.001.

Gogou, A., I. Bouloubassi, V. Lykousis, M. Arnaboldi, P. Gaitani, and P. A. Meyers (2007), Organic geochemical evidence of abrupt late glacial-Holocene climate changes in the North Aegean Sea, *Palaeogeogr. Palaeoclimatol. Palaeoecol.*, *256*, 1–20, doi:10.1016/j.palaeo.2007.08.002.

Hemleben, C., M. Spindler, and R. O. Anderson (1989), *Modern Planktonic Foraminifera*, Springer, Heidelberg, Germany.

Hoogakker, B. A. A., G. Klinkhammer, H. Elderfield, E. J. Rohling, and C. Hayward (2009), Mg/Ca paleothermometry in high salinity environments, *Earth Planet. Sci. Lett.*, *284*, 583–589, doi:10.1016/j.epsl.2009.05.027.

Hover, V. C., L. M. Walter, and D. R. Peacor (2001), Early marine diagenesis of biogenic aragonite and Mg-calcite: New constraints from high-resolution STEM and AEM analyses of modern platform carbonates, *Chem. Geol.*, *175*, 221–248.

Katsouras, G., A. Gogou, I. Bouloubassi, K.-C. Emeis, M. Triantaphyllou, G. Roussakis, and V. Lykousis (2010), Organic carbon distribution and isotopic composition in three records from the eastern Mediterranean Sea during the Holocene, *Org. Geochem.*, *41*, 935–939, doi:10.1016/j.orggeochem.2010.04.008.

Kısakürek, B., A. Eisenhauer, F. Böhm, D. Garbe-Schönberg, and J. Erez (2008), Controls on shell Mg/Ca and Sr/Ca in cultured planktonic foraminiferan, *Globigerinoides ruber* (white), *Earth Planet. Sci. Lett.*, *273*(3–4), 260–269, doi:10.1016/j.epsl.2008.06.026.

Klein, B., W. Roether, B. B. Manca, D. Bregant, V. Beitzel, V. Kovasevic, and A. Luchetta (1999), The large deep water transient in the eastern Mediterranean, *Deep Sea Res., Part I*, *46*, 371–414, doi:10.1016/S0967-0637(98)00075-2.

Lea, D. W., D. K. Pak, and H. J. Spero (2000), Climate impact of late quaternary equatorial pacific sea surface temperature variations, *Science*, *289*(5485), 1719–1724, doi:10.1126/science.289.5485.1719.

Lykousis, V., et al. (2002), Major outputs of the recent multidisciplinary biogeochemical researches undertaken in the Aegean Sea, *J. Mar. Syst.*, *33–34*, 313–334.

Marino, G., E. J. Rohling, F. Sangiorgi, A. Hayes, J. L. Casford, A. F. Lotter, M. Kucera, and H. Brinkhuis (2009), Early and middle Holocene in the Aegean Sea: Interplay between high and low latitude climate variability, *Quat. Sci. Rev.*, *28*, 3246–3262, doi:10.1016/j.quascirev.2009.08.011.

Mathien-Blard, E., and F. Bassinot (2009), Salinity bias on the foraminifera Mg/Ca thermometry: Correction procedure and implications for past ocean hydrographic reconstructions, *Geochem. Geophys. Geosyst.*, *10*, Q12011, doi:10.1029/2008GC002353.

Melim, L. A., H. Westphal, P. K. Swart, G. P. Eberli, and A. Munnecke (2002), Questioning carbonate diagenetic paradigms: Evidence from the Neogene of the Bahamas, *Mar. Geol.*, *185*, 27–53, doi:10.1016/S0025-3227(01)00289-4.

Morse, J. W., F. J. Millero, V. Thurmond, E. Brown, and H. G. Ostlund (1984), The carbonate chemistry of Grand Bahama Bank waters: After 18 years another look, *J. Geophys. Res.*, *89*, 3604–3614, doi:10.1029/JC089iC03p03604.

Morse, J. W., Q. Wang, and M. Y. Tsio (1997), Influences of temperature and Mg:Ca ratio on $CaCO_3$ precipitates from sea water, *Geology*, *25*, 85–87, doi:10.1130/0091-7613(1997)025<0085:IOTAMC>2.3.CO;2.

Mucci, A. (1987), Influence of temperature on the composition of magnesian calcite overgrowths precipitated from seawater, *Geochim. Cosmochim. Acta*, *51*, 1977–1984, doi:10.1016/0016-7037(87)90186-4.

Ni, Y., G. L. Foster, T. Bailey, T. Elliott, D. N. Schmidt, P. Pearson, B. Haley, and C. Coath (2007), A core top assessment of proxies for the ocean carbonate system in surface-dwelling foraminifers, *Paleoceanography*, *22*, PA3212, doi:10.1029/2006PA001337.

Poulos, S. E., P. G. Drakopoulos, and M. B. Collins (1997), Seasonal variability in sea surface oceanographic conditions in the Aegean Sea (eastern Mediterranean): An overview, *J. Mar. Syst.*, *13*, 225–244, doi:10.1016/S0924-7963(96)00113-3.

Pujol, C., and C. Vergnaud-Grazzini (1995), Distribution patterns of live planktic foraminifers as related to regional hydrography and productive systems of the Mediterranean Sea, *Mar. Micropaleontol.*, *25*, 187–217, doi:10.1016/0377-8398(95)00002-I.

Raitzsch, M., A. Duenas-Bohórquez, G.-J. Reichart, L. J. de Nooijer, and T. Bickert (2010), Incorporation of Mg and Sr in calcite of cultured benthic foraminifera: Impact of calcium concentration and associated calcite saturation state, *Biogeosciences*, *7*, 869–881, doi:10.5194/bg-7-869-2010.

Regenberg, M., D. Nürnberg, J. Garbe-Schönfeld, and G.-J. Reichart (2007), Early diagenetic overprint in Caribbean sediment cores and its effect on the geochemical composition of planktonic foraminifera, *Biogeosciences*, *4*, 957–973, doi:10.5194/bg-4-957-2007.

Rohling, E. J., et al. (2002), African monsoon variability during the previous interglacial maximum, *Earth Planet. Sci. Lett.*, *202*, 61–75.

Rosenthal, Y., et al. (2004), Interlaboratory comparison study of Mg/Ca and Sr/Ca measurements in planktonic foraminifera for paleoceanographic research, *Geochem. Geophys. Geosyst.*, *5*, Q04D09, doi:10.1029/2003GC000650.

Roussakis, G., A. P. Karageorgis, N. Conispoliatis, and V. Lykousis (2004), Last glacial-Holocene sediment sequences in N. Aegean basins: Structure, accumulation rates and clay mineral distribution, *Geo Mar. Lett.*, *24*, 97–111, doi:10.1007/s00367-004-0167-0.

Russell, A. D., B. Hoenisch, H. J. Spero, and D. W. Lea (2004), Effects of seawater carbonate ion concentration and temperature on shell U, Mg, and Sr in cultured planktonic foraminifera, *Geochim. Cosmochim. Acta*, *68*(21), 4347–4361, doi:10.1016/j.gca.2004.03.013.

Schneider, A., D. W. R. Wallace, and A. Körtzinger (2007), Alkalinity of the Mediterranean Sea, *Geophys. Res. Lett.*, *34*, L15608, doi:10.1029/2006GL028842.

Sexton, P. F., P. A. Wilson, and P. N. Pearson (2006), Palaeoecology of late middle Eocene planktic foraminifera and evolutionary implications, *Mar. Micropaleontol.*, *60*, 1–16, doi:10.1016/j.marmicro.2006.02.006.

Thomson, J., D. Crudeli, G. J. de Lange, C. P. Slomp, E. Erba, C. Corselli, and S. E. Calvert (2004), *Florisphaera profunda* and the origin and diagenesis of carbonate phases in eastern Mediterranean sapropel units, *Paleoceanography*, *19*, PA3003, doi:10.1029/2003PA000976.

Triantaphyllou, M. V., et al. (2009a), Late Glacial-Holocene ecostratigraphy of the south-eastern Aegean Sea, based on plankton and pollen assemblages, *Geo Mar. Lett.*, *29*, 249–267, doi:10.1007/s00367-009-0139-5.

Triantaphyllou, M. V., et al. (2009b), Late Glacial-Holocene climate variability at the south-eastern margin of the Aegean Sea, *Mar. Geol.*, *266*, 182–197, doi:10.1016/j.margeo.2009.08.005.

Triantaphyllou, M. V., M. Dimiza, E. Krasakopoulou, E. Malinverno, V. Lianou, and E. Souvermezoglou (2010), Seasonal variation in *Emiliania huxlei* coccolith morphology and calcification in the Aegean Sea (eastern Mediterranean), *Geobios*, *43*, 99–110, doi:10.1016/j.geobios.2009.09.002.

van Raden, U. J., J. Groeneveld, M. Raitzsch, and M. Kucera (2011), Mg/Ca in the planktonic foraminifera *Globorotalia inflata* and *Globigerinoides bulloides* from Western Mediterranean plankton tow and core top samples, *Mar. Micropaleontol.*, *78*, 101–112, doi:10.1016/j.marmicro.2010.11.002.

Zhang, Y., and R. A. Dawe (2000), Influence of Mg^{2+} on the kinetics of calcite precipitation and calcite crystal morphology, *Chem. Geol.*, *163*, 129–138.

Zhong, S., and A. Mucci (1989), Calcite and aragonite precipitation from seawater of various solutions of various salinities: Precipitation rates and overgrowth compositions, *Chem. Geol.*, *78*, 283–299, doi:10.1016/0009-2541(89)90064-8.